J Infrared Milli Terahz Waves (2017) 38:1316–1320
DOI 10.1007/s10762-017-0428-4

Communications with THz Waves: Switching Data Between Two Waveguides

J. Ma[1] · M. Weidenbach[2] · R. Guo[2] · M. Koch[2] · D. M. Mittleman[1]

Received: 5 July 2017 / Accepted: 30 July 2017 /
Published online: 7 August 2017

1 Introduction

Wireless communication with terahertz (THz) carrier waves is a rapidly developing field [1, 2], with considerable effort being devoted to demonstrations of high-data rate links [3–5] as well as devices for transporting [6, 7] and manipulating [8–11] THz signals. Dielectric waveguides represent one important platform for both signal transport and signal processing. With relatively low absorption losses and considerable design flexibility, dielectric structures offer great promise as both active and passive devices. One particular advantage is the possibility of fabrication by 3D printing, which offers a low-cost and highly versatile method for production of nearly arbitrary waveguiding structures [12, 13]. For example, Weidenbach et al. [14] have recently demonstrated a suite of 3D printed waveguide designs with low loss in the THz range, including a fixed power splitter and a variable waveguide splitter based on evanescent wave coupling [15] between two parallel dielectric waveguides. Here, we explore such a variable coupler using a modulated data stream at ~ 196 GHz.

2 Experimental Setup and Results

The waveguides are printed out of polystyrene (PS), a material which is reasonably transparent at THz frequencies with a nearly frequency-independent refractive index of 1.56. PS can be printed using a Ultimaker Original 3D printer [13]. We have used COMSOL Multiphysics 5.2 to optimize the waveguide dimensions for single-mode operation. The printed waveguide has a square cross section of size 0.8 mm by 0.8 mm, which assures single-mode operation in the

✉ D. M. Mittleman
daniel_mittleman@brown.edu

[1] School of Engineering, Brown University, 184 Hope Street, Providence, RI 02912, USA

[2] Department of Physics and Materials Sciences Center, Philipps-Universität Marburg, Renthof 5, 35032 Marburg, Germany

frequency range of interest. As shown in Fig. 1, it consists of a 90° turn followed by a coupling section in which two identical waveguides run parallel to each other with a mechanically variable spacing between them. The 90° bend prevents direct free-space coupling between the transmitter and receiver [14], and its bending loss is small for a curvature radius r = 20 mm. The coupling region has a nominal length of 60 mm, although the effective coupling length is somewhat larger due to non-zero coupling even in the curved regions [14]. Using numerical simulation, we determine that the effective refractive index of the fundamental mode of this waveguide at 196 GHz is 1.229.

For the data transmission experiments, we used a source based on a frequency multiplier chain (Virginia Diodes), which up-converts a modulated baseband signal to 196 GHz producing about 60 mW of power at the output of the horn antenna. We generate a pseudo-random bit pattern to modulate this carrier wave at 1 Gb/s via amplitude shift keying (ASK) modulation. We detect the signal using a zero-biased Schottky diode intensity detector. The Schottky signal is amplified to drive a bit error rate (BER) tester (Anritsu MP1764A) for real-time signal analysis. Unlike in the previous study [14], the waveguides are not inserted into the horn antennas, but rather are held approximately 7.25 mm outside of the ends of the horns at the transmitter side and 2 mm at the receiver end (see Fig. 1). This arrangement artificially reduces the coupling efficiency in order to avoid saturating the detector, thus optimizes the signal-to-noise ratio of the measurement. We estimate that the input coupling efficiency from the transmitter horn to the waveguide is −36 dB. The maximum power detected at each of the two waveguide outputs is −22 dBm, which is smaller than the generated power due to this finite coupling efficiency as well as to the waveguide bend loss and to other smaller loss mechanisms such as absorption in the PS and surface roughness effects.

Figure 2 shows typical results for an input wave of 196 GHz with a data rate of 1 Gb/s. Figure 2a shows the power at the two waveguide outputs, which varies periodically between P_2 (black symbols) and P_3 (blue symbols) as the space between the two parallel waveguides is mechanically increased. In the limit of large separation, the coupling between the two waveguides is negligible, and all the power emerges

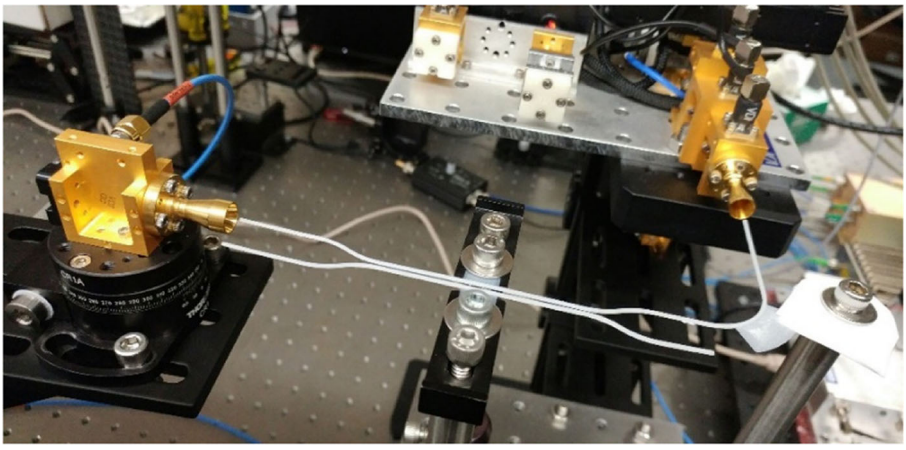

Fig. 1 Top view of the experimental setup. Horn antennas with a full 3 dB beamwidth of 13-degrees are attached on transmitter (upper right) and receiver (left). Waveguides are mounted on a linear stage by thin supporters, so that the active area of the waveguides are effectively suspended in air. In this photo, the receiver horn is positioned at the primary (P_2) output; in the measurements, it can also be positioned in front of the secondary (P_3) output

from P_2. As observed in [14], this oscillatory behavior can be understood in terms of the difference in the propagation constants of the even and odd waveguide modes, as:

$$P_2 = P_1 \cdot \cos^2\left(\frac{\beta_{even} - \beta_{odd}}{2} \cdot z\right) \tag{1}$$

and

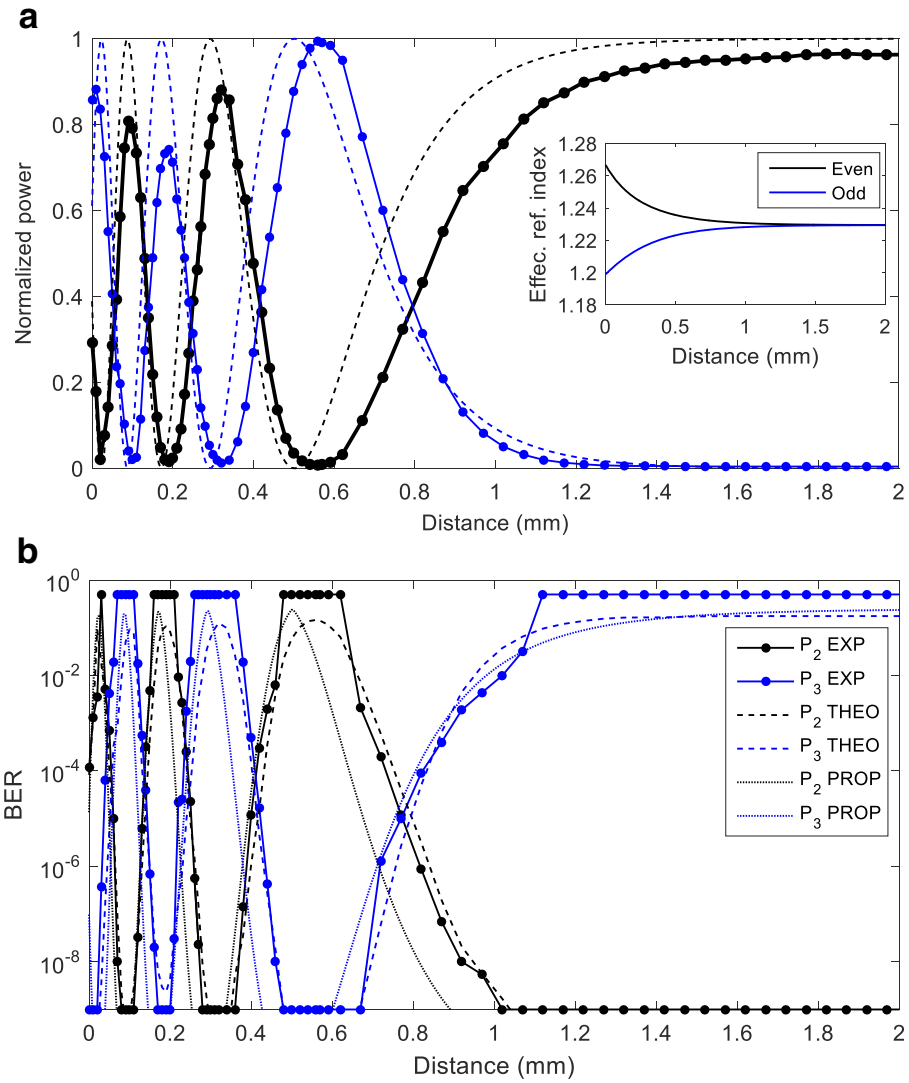

Fig. 2 **a** Power variation at the output ports as a function of the separation between the primary (P_2, shown in black) and secondary (P_3, shown in blue) waveguides. Solid lines with solid circles show experimental measurements; dashed lines show predictions based on numerical simulations. Inset: effective refractive indices for even and odd modes as a function of separation. Both modes converge to the same value of 1.229 when the separation is large. **b** Corresponding BER variation versus separation distance between the two waveguides. Dashed lines show the predictions made using the power measurements in (**a**) while the dotted lines show the predictions made using the simulated values displayed in (**a**)

$$P_3 = P_1 \cdot \sin^2\left(\frac{\beta_{even} - \beta_{odd}}{2} \cdot z\right) \quad (2)$$

where P_1 is the input power to the coupling region, and where z = 60 mm is the length of the coupling region. The propagation constant relates to effective refractive index by $\beta = 2\pi n/\lambda$ with λ as the wavelength in free space and n as the effective index of the mode. β_{even} and β_{odd} are propagation constants for the even (symmetric) and odd (antisymmetric) modes of the coupling region (i.e., the super-modes). The fact that $\beta_{\text{even}} \neq \beta_{\text{odd}}$ leads to mode beating as a function of waveguide separation, and therefore, energy transfer between the two branches. In the inset of Fig. 2a, we show the effective indices for the even and odd modes, extracted from numerical simulations for different values of the distance between the two parallel waveguide sections. The dashed lines in Fig. 2a show predicted values for P_2 and P_3, using these simulated values for the effective index. We note a slight discrepancy between simulation and experiment, which we attribute to structural imperfections of the device such as surface roughness which is inherent to 3D printed structures.

The corresponding BER performance is illustrated in Fig. 2b. The BER at output port 2 (port 3) can be computed from the signal-to-noise, which is directly proportional to P_2 (P_3), according to

$$BER_{port\ j} = \frac{1}{2} e^{-P_j / 4N} \cdot \frac{1}{2} erfc\left(\sqrt{\frac{P_j}{2N}}\right) \quad (3)$$

Here, N is noise power composed of thermal noise and additional noise defined by noise figure. As a result, the oscillatory power output also results in an oscillatory behavior for the BER, in each output channel. With the aforementioned input power, we observe that the signal at the output achieves error-free performance (BER < 10^{-9}) multiple times as the waveguide separation varies from zero to its maximum value. Indeed, there are numerous points where the BER in both channels is simultaneously low enough (less than 2×10^{-3}) for error-free transmission with forward error correction. This result establishes the fact that these 3D printed waveguide couplers have sufficient quality to be used as tunable signal processing elements in real systems.

3 Conclusions

We have demonstrated the coupling behavior of two identical and parallel dielectric waveguides made out of 3D printed polystyrene in a real-time THz wireless link. Due to the low loss and low dispersion of these waveguide structures, the BER at both the straight and cross-coupled waveguide outputs can readily achieve error-free performance at 1 Gb/s. Even higher data rates are readily possible, limited ultimately by the very small waveguide dispersion which will cause inter-symbol interference at extremely high data rates. This highly flexible approach holds great promise for applications in THz signal processing.

Acknowledgments This work was supported in part by the US National Science Foundation and the W.M. Keck Foundation.

References

1. R. Piesiewicz, T. Kleine-Ostmann, N. Krumbholz, D. Mittleman, M. Koch, J. Schöbel, and T. Kürner. Short-range ultra broadband terahertz communications: concept and perspectives, IEEE Antennas & Propag. Mag. 49, 24–39 (2007).
2. T. Kleine-Ostmann, and T. Nagatsuma. A review on terahertz communications research, J. Infrared Millim. Terahertz Waves 32, 143–171 (2011).
3. I. Kallfass, F. Boes, T. Messinger, J. Antes, A. Inam, U. Lewark, A. Tessmann, and R. Henneberger, 64 Gbit/s transmission over 850 m fixed wireless link at 240 GHz carrier frequency," J. Infrared Millim. Terahertz Waves 36, 221–233 (2015).
4. X. Yu, S. Jia, H. Hu, M. Galili, T. Morioka, P. U. Jepsen, and L. K. Oxenløwe, 160 Gbit/s photonics wireless transmission in the 300-500 GHz band, APL Photon. 1, 081301 (2016).
5. H.-J. Song, K. Ajito, Y. Muramoto, A. Wakatsuki, T. Nagatsuma and N. Kukutsu, 24 Gbit/s data transmission in 300 GHz band for future terahertz communications, Electron. Lett. 48, 953–954 (2012).
6. M. Mbonye, R. Mendis, and D. M. Mittleman, Measuring TE_1 mode losses in terahertz parallel-plate waveguides, J. Infrared Millim. Terahertz Waves 34, 416–422 (2013).
7. H. Bao, K. Nielsen, H. K. Rasmussen, P. U. Jepsen, and O. Bang. Design and optimization of mechanically down-doped terahertz fiber directional couplers, Opt. Express 22, 9486–9497 (2014).
8. T. Kleine-Ostmann, K. Pierz, G. Hein, P. Dawson, and M. Koch. Audio signal transmission over THz communication channel using semiconductor modulator, Electron. Lett. 40, 124–126 (2004).
9. K. Reichel, R. Mendis, and D. M. Mittleman, A broadband terahertz waveguide T-junction variable power splitter, Sci. Rep. 6, 28925 (2016).
10. N. J. Karl, R. W. McKinney, Y. Monnai, R. Mendis, and D. M. Mittleman, Frequency-division multiplexing in the terahertz range using a leaky wave antenna, Nature Photon. 9, 717–720 (2015).
11. J. Ma, N. J. Karl, S. Bretin, G. Ducournau, and D. M. Mittleman. Frequency-division multiplexer/demultiplexer for terahertz wireless links, Nature Commun., doi:10.1038/s41467-017-00877-x (2017).
12. J. Liu, R. Mendis, and D. M. Mittleman,A Maxwell's fish eye lens for the terahertz region, Appl. Phys. Lett. 103, 031104 (2013).
13. S. F. Busch, M. Weidenbach, M. Fey, F. Schäfer, T. Probst, and M. Koch. Optical properties of 3D printable plastics in the THz regime and their application for 3D printed THz optics, J. Infrared Millim. Terahertz Waves 35, 993–997 (2014).
14. M. Weidenbach, D. Jahn, A. Rehn, S. F. Busch, F. Beltrán-Mejía, J. C. Balzer, and M. Koch. 3D printed dielectric rectangular waveguides, splitters and couplers for 120 GHz, Opt. Express 24, 28968–28976 (2016).
15. K. Reichel, N. Sakoda, R. Mendis, and D. M. Mittleman, Evanescent wave coupling in terahertz waveguide arrays,, Opt. Express 21, 17249–17255 (2013).